Impacts of relative permeability hysteresis, wettability, and injection/withdrawal schemes on underground hydrogen storage in saline aquifers

Impacts of relative permeability hysteresis, wettability, and injection/withdrawal schemes on underground hydrogen storage in saline aquifers

Bin Pan [1], Kai Liu [1], Bo Ren [2], Mingshan Zhang [3], Yang Ju [4], Jianwei Gu [5], Xueying Zhang [6], Christopher R. Clarkson [7], Katriona Edlmann [8], Weiyao Zhu [1*], and Stefan Iglauer [9,10]

[1]*School of Civil and Resource Engineering, University of Science and Technology Beijing, No. 30, Xueyuan Road, Beijing, 10083, China*

[2]*Bureau of Economic Geology, The University of Texas at Austin, 10611 Exploration Way, Austin, TX 78758, US*

[3]*Key Laboratory of Ministry of Education on Safe Mining of Deep Metal Mines, School of Resources and Civil Engineering, Northeastern University, Shenyang 110819, China*

[4]*State Key Laboratory of Coal Resources and Safe Mining, China University of Mining and Technology at Beijing, D11 Xueyuan Road, Beijing 100083, China*

[5]*School of Petroleum Engineering, China University of Petroleum (East China), No. 66, Changjiang West Road, Qingdao, China*

[6]*PetroChina Huabei Oilfield Company, Hebei, 062552, China*

[7]*Department of Geoscience, University of Calgary, Calgary, AB, T2N 1N4, Canada*

[8]*School of Geosciences, University of Edinburgh, Grant Institute, Edinburgh, UK*

[9]*School of Engineering, Edith Cowan University, 270 Joondalup Drive, Joondalup, Australia*

[10]*Centre for Sustainable Energy and Resources, Edith Cowan University, 270 Joondalup Drive, Joondalup, Australia*

Abstract

Underground hydrogen storage (UHS) is a key strategy in the implementation of a large-scale hydrogen (H_2) economy and promotion of renewable energy development/utilization. For UHS in water-wet saline aquifers, H_2 displaces *in-situ* brine during injection; during well shut-in and H_2 withdrawal, brine imbibes back into the flow paths where it displaces some H_2. These processes are influenced by H_2-brine transport physics, H_2-brine-rock interactions and injection/withdrawal schemes, which, in turn, determine H_2 storage capacities and injection/withdrawal efficiency. However, these effects are poorly understood. Therefore, this work focuses on the impact of relative permeability hysteresis (RPH), wettability, and H_2 withdrawal rate on UHS performance in a saline aquifer. Furthermore, differences between UHS and CO_2 geo-storage (CGS) are examined.

The primary findings include: 1) RPH results in a smaller H_2 withdrawal factor (H_{2-WF}), but a larger H_2 withdrawal purity (H_{2-WP}); 2) H_{2-WF} increases with rock hydrophobicity, while H_{2-WP} is mostly insensitive to rock wettability; 3) under similar storage conditions, H_{2-WF} and H_{2-WP} are approximately 10% less than CO_{2-WF} and CO_{2-WP}.

These insights demonstrate the significance of RPH and rock wettability on UHS performance and provides guidance on H_2 injection/withdrawal scheme optimization. This study aids in the implementation of an industry-scale hydrogen economy.

Keywords: Underground hydrogen storage; Saline aquifers; Relative permeability hysteresis; Wettability; Injection/withdrawal scheme.

1. Introduction

Commercial development of renewable and sustainable energy resources are required to accelerate energy transition, mitigate global warming, and accomplish carbon neutrality [1–3]. However, these energy resources (e.g., wind, solar, and tide) are time-, season-, weather- and/or region- dependent, which limits their stability, reliability and large-scale economic implementation [4–6]. To overcome these drawbacks, underground hydrogen storage (UHS) is considered as a promising solution [7–11]. When energy supply is larger than energy demand, excess renewable and sustainable energy can be converted to hydrogen (H_2) through water electrolysis as a green energy carrier, and the H_2 can be injected into the subsurface for storage; when energy demand is high, H_2 can be withdrawn again from the subsurface for usage [12–17]. Potential subsurface storage sites include deep coal seams [18,19], depleted hydrocarbon reservoirs [20,21], aquifers [22,23] and salt caverns [15,24]. Salt caverns are suitable for frequent cyclic H_2 injection and withdrawal, but salt cavern storage capacities are usually small (around 50×10^4 Sm^3 [15,24,25]). Depleted hydrocarbon reservoirs are often well characterized with the necessary geological information, and substantial surface/subsurface infrastructure are in place [20,21]. However, microbial activity may be high, which causes both serious H_2 loss and H_2 purity reduction (e.g. via the reactions $C_2H_6 + H_2 \rightarrow 2\,CH_4$ or $H_2 + S \rightarrow H_2S$

[8,16,26]). In contrast, saline aquifers have the largest storage capacity and relatively weak microbial reactions, and thus attract significant attention [7,27]. Heinemann et al. [7] discussed the scientific challenges to enabling large-scale hydrogen storage in saline reservoirs while Pan et al. [27] reviewed all available experimental data related to UHS in saline aquifers.

Numerical simulation is a cost-effective and rapid method for large-scale UHS evaluation, which should be conducted prior to field-scale pilot tests. Pfeiffer et al. [28,29] used numerical simulations to predict UHS performance in the Rhaetian deposit, Germany, and the results demonstrated that up to 7700 $\times 10^4$ Sm^3 (equal to 245 MW electricity) could be stored. Feldmann et al. [30] simulated 5 years of continuous H_2 injection and subsequent 5 years of seasonal cyclic H_2 injection/withdrawal into a depleted gas reservoir; the authors found that the H_2 withdrawal purity (H_{2-WP}) and withdrawal factor (H_{2-WF}) reached 82% - 85% and 39%, respectively. Sainz-Garcia et al. [22] conducted a three-dimensional multiphase numerical simulation for three annual H_2 injection/withdrawal cycles in Castilla-Leon, Spain. The stored H_2 (67400 $\times 10^4$ Sm^3) was able to supply 15% of the electric consumption for a population of 175,000 over 3 months. Additionally, Lubon and Tarkowski [23] utilized numerical simulations to predict seasonal H_2 cyclic injection/withdrawal scenarios in a deep aquifer at Suliszewo, Poland - it was discovered that water coning was the main obstacle for UHS performance. Recently, Heinemann et al. [11] investigated the role of cushion gas for H_2 injection and withdrawal in saline aquifers, demonstrating that the produced

H_2 was equal to 1.625 TWH from a three dimensional anticline reservoir model with the ratio of cushion gas to working gas at 1.27 [11].

In the above-mentioned UHS simulations, either CO_2-brine relative permeability curves were used as input parameters [11,28,29], or H_2-brine relative permeability hysteresis (RPH) was not considered [22,23,30] (though CO_2 RPH strongly influences capillary CO_2 trapping in saline reservoirs in CGS schemes [31]). To mitigate this uncertainty, and to address the fact that H_2 is a very different molecule than CH_4 or CO_2 [27,32], UHS reservoir simulations with real H_2 input parameters and H_2 transport physics are required.

Therefore herein, the impact of RPH, rock-H_2 wettability, and injection/withdrawal schemes on UHS performance in saline aquifers is systematically evaluated. Further, the acquired UHS results are compared with CGS data. This work will provide important information supporting large-scale UHS implementation and the decarbonization of energy supply chains.

2. Methodology

2.1 Geological model

The commercial reservoir simulator IMEX from Computer Modelling Group (CMG) was used to simulate UHS in a synthetic PUNQ-S3 geological model. This simulation is based on the classic black-oil model following the mass conservation principles [33]. PUNQ-S3 is a three-dimensional, geometrically complicated and heterogeneous geological model (a central dome + 5 layers of sand/shale) [34]. This

model was previously used for oil production forecasting [34] and CO_2 geo-storage simulation [31]. The average aquifer thickness is 15 m, and the entire domain is discretized into 19 × 28 × 5 grid blocks (1761 of them active). Each cell has a length of 180 m in the horizontal direction. The average horizontal permeability and porosity are 100 mD and 0.2, respectively, with their spatial distributions shown in **Figure 1**.

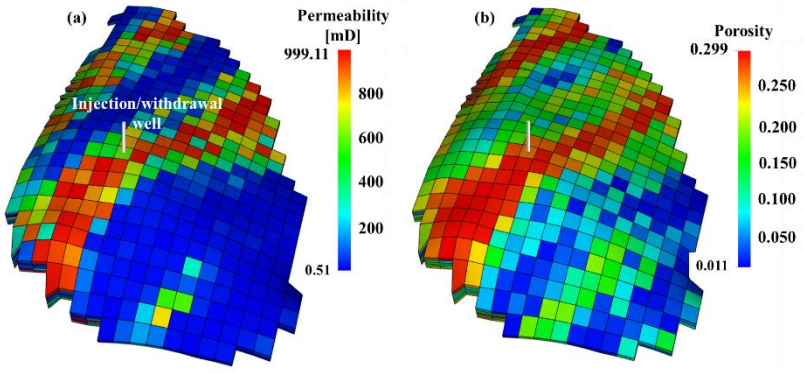

Figure 1. (a) Horizontal permeability and (b) porosity distributions in the PUNQ-S3 geological model (Modified after [31]). For simplicity, only one well was used for gas injection and withdrawal.

A single well was drilled at the structurally highest location for gas injection and withdrawal. Similar to [31], the pore volume around the geological boundaries is set ~1000 times larger than the area of interest so that *in-situ* brine could be displaced during the gas injection; the displaced brine is imbibed back again during well shut-in (in case of water-wet rock) and simultaneously pumped out of the subsurface with gas during gas withdrawal.

2.2 Input parameters

Information about H_2 density, H_2 viscosity and H_2 expansion factor at UHS conditions are tabulated in **Table 1**. Currently, only one H_2-brine relative permeability

curve was measured for the process of H_2 injection into a brine saturated water-wet sandstone [35] (**Figure 2**). Using pore network modelling, H_2-brine relative permeability curves (for drainage and imbibition) were also predicted for additional rock wettabilities [i.e., brine contact angles (θ) of 51° and 83°] [36] (**Figure 2**). Information about CO_2 properties and relative permeability curves (which were collected from previous literature [31]) are not shown here for simplicity.

Table 1. H_2 properties at 40 °C and various pressures (compiled from [7,27]).

Pressure [MPa]	Density [kg/m^3]	Expansion factor [-]	Viscosity [mPa·s]
0.1	0.089	1	0.0092
10	8	89.9	0.0094
20	14	157.3	0.0096
30	20	224.7	0.0098
40	24	269.7	0.01
50	29	325.8	0.0104

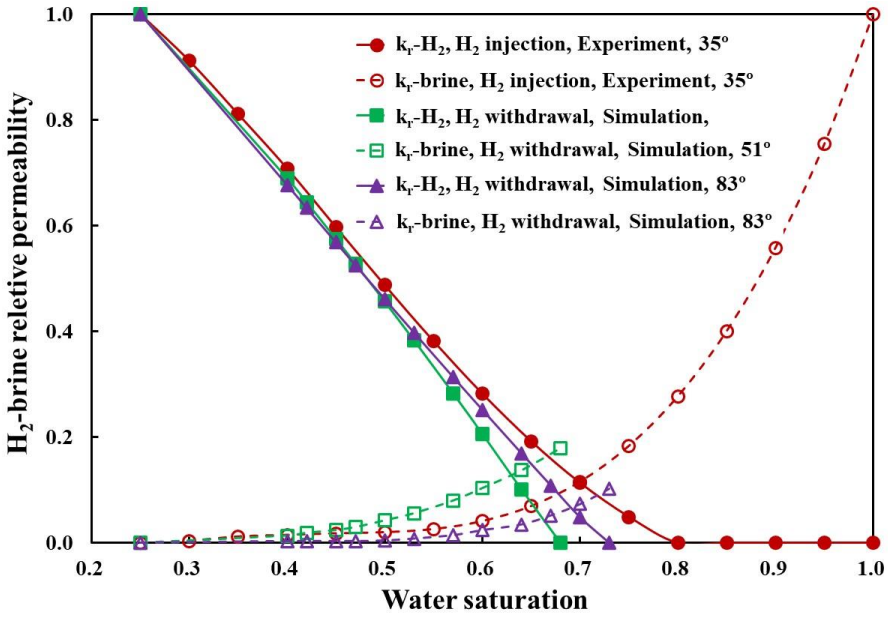

Figure 2. H_2-brine relative permeability curves (modified after [35,36]; curve fitting was conducted to smooth the raw experimental and simulation data based on the least squares method). Experimental data is from [30]; simulated curves using pore network modeling are from [31].

2.3 Simulation scenarios

Four separate scenarios were simulated to explore the impact of RPH, rock wettability, and injection/withdrawal scheme on UHS performance, **Table 2**. In addition, two scenarios were simulated for CGS to provide a comparison.

Table 2. Scenarios simulated in this work (NA means that CO_2 wettability was unknown in the simulations).

Gas	Case	Relative permeability hysteresis	Wettability	Injection/withdrawal scheme
H_2	1 (base case)	No	35º	a. Injection at 50×10^4 Sm^3/day for 9 months; well shut-in for 3 months b. Withdrawal at 100×10^4 Sm^3/day for 3 months; injection at 50×10^4 Sm^3/day for 6 months; well shut-in for 3 months c. Repeat b for 4 cycles
	2	Yes	51°	Same as case 1
	3	Yes	83°	Same as above
	4	Yes	51°	a. Injection at 50×10^4 Sm^3/day for 9 months; well shut-in for 3 months b. Withdrawal at 200×10^4 Sm^3/day for 3 months; injection at 50×10^4 Sm^3/day for 6 months; well shut-in for 3 months c. Repeat b for 4 cycles
CO_2	5 (base case)	No	NA	a. Injection at 50×10^4 Sm^3/day for 9 months; well shut-in for 3 months b. Withdrawal at 100×10^4 Sm^3/day for 3 months; injection at 50×10^4 Sm^3/day for 6 months; well shut-in for 3 months c. Repeat b for 4 cycles
	6	Yes	NA	Same as case 5

3 Results and discussion

3.1 Impact of relative permeability hysteresis and wettability

For UHS, H_2 injection into a water-wet aquifer is dominated by the forced drainage (of the resident formation water), while H_2 withdrawal is dominated by the spontaneous and forced imbibition [37,38]. Therefore, it is necessary to assess the impact of RPH and rock wettability on UHS performance.

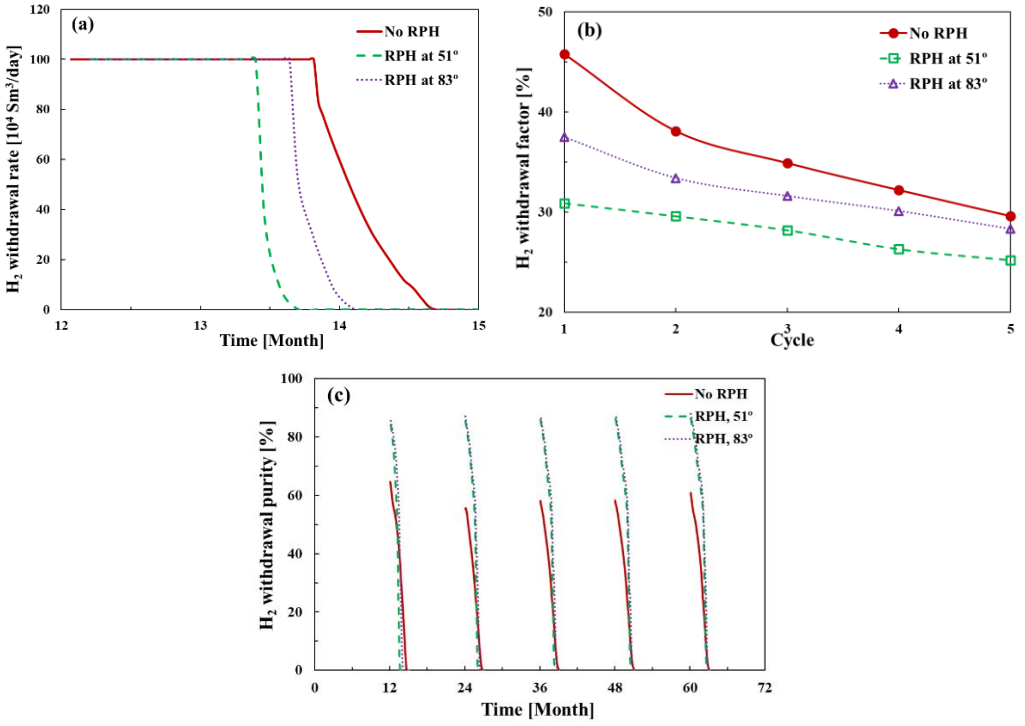

Figure 3. Effect of relative permeability hysteresis and rock wettability on the (a) actual H_2 withdrawal rate during the 1st withdrawal cycle, (b) H_2 withdrawal factor (the ratio of the accumulated H_2 withdrawal volume during a specific H_2 withdrawal cycle to the total H_2 in-place volume prior to this withdrawal cycle) and (c) H_2 withdrawal purity (the ratio of H_2 withdrawal mass to water production mass) at the prescribed withdrawal rate of 100×10^4 Sm^3/day).

RPH and a strongly water-wet state cause the actual H_2 withdrawal rate (H_{2-WR}) to deviate from the prescribed H_{2-WR} value and to reach zero earlier, **Figure 3(a)**. During the 1st H_2 withdrawal cycle, the actual H_{2-WR} started to deviate from the prescribed 100×10^4 Sm^3/day on the 54th, 36th and 45th day, while it reached zero on the 81st, 49th and 62nd day, for the case of no RPH, case with RPH at $\theta = 51°$, and the case with RPH at $\theta = 83°$, respectively. Further, by the end of each withdrawal cycle, the H_2 withdrawal factor (H_{2-WF}, the ratio of the accumulated H_2 withdrawal volume during a specific H_2 withdrawal cycle to the total H_2 in-place volume prior to this withdrawal cycle) follows the order: case with no RPH > case with RPH at $\theta = 83° >$ case with RPH at $\theta = 51°$. H_{2-WF} was 38%, 33% and 30%, respectively for the above-mentioned three scenarios at the end of the 2nd withdrawal cycle, **Figure 3(b)**. Moreover, at the beginning of each H_2 withdrawal cycle, RPH causes a larger H_2 withdrawal purity (H_{2-WP}, the ratio of H_2 withdrawal mass to water production mass) than without RPH (e.g., 86% - 88% versus 55% - 65%), though the wettability impact is insignificant, **Figure 3(c)**. In addition, with the H_2 withdrawal cycle increase, H_{2-WF} decreased at the end of each cycle of withdrawal, while H_{2-WP} increased at the beginning of each cycle of withdrawal, **Figure 3(b)** and **(c)**, consistent with the previous literature study [28].

Note that RPH and rock wettability influence pore-scale gas-brine two phase flow characteristics and therefore determine reservoir-scale gas injection/withdrawal efficiency [38–43]. In the absence of RPH, the injected gas exists as a continuous gas plume, and capillary trapping is relatively weak [31]. If RPH is present, the trailing

edges of the gas plumes tend to convert into discontinuous phases, and capillary trapping are relatively strong (which is favorable for CGS because of reduced leakage risk) – however, it is unfavorable for UHS because of the more difficult gas re-mobilization [27]. Therefore, H_{2-WF} was higher in the absence of RPH. Further, a more water-wet state leads to more snap off events [44,45], and therefore a more serious H_2 loss and a smaller H_{2-WF}. Moreover, during well shut-in, discontinuous H_2 bubbles can exert strong resistance for the spontaneous imbibition of *in-situ* formation brine [46,47] – therefore, if RPH is present, the initial H_2 concentration is higher around the wellbore region (which again results in a larger H_{2-WP} at the beginning of each H_2 withdrawal cycle). The observed H_{2-WF} and H_{2-WP} response to the withdrawal cycle is because 1) at the end of each H_2 injection cycle, more H_2 will be in place than the earlier injection cycle; and 2) at the end of each H_2 withdrawal cycle, more H_2 will be lost to the subsurface than the earlier withdrawal cycle [28].

3.2 Impact of H_2 withdrawal rate

To operate a field-scale UHS project efficiently, the H_2 injection/withdrawal scheme [7] should be optimized, especially H_{2-WR}. Therefore, the impact of H_{2-WR} on UHS performance was investigated in this section.

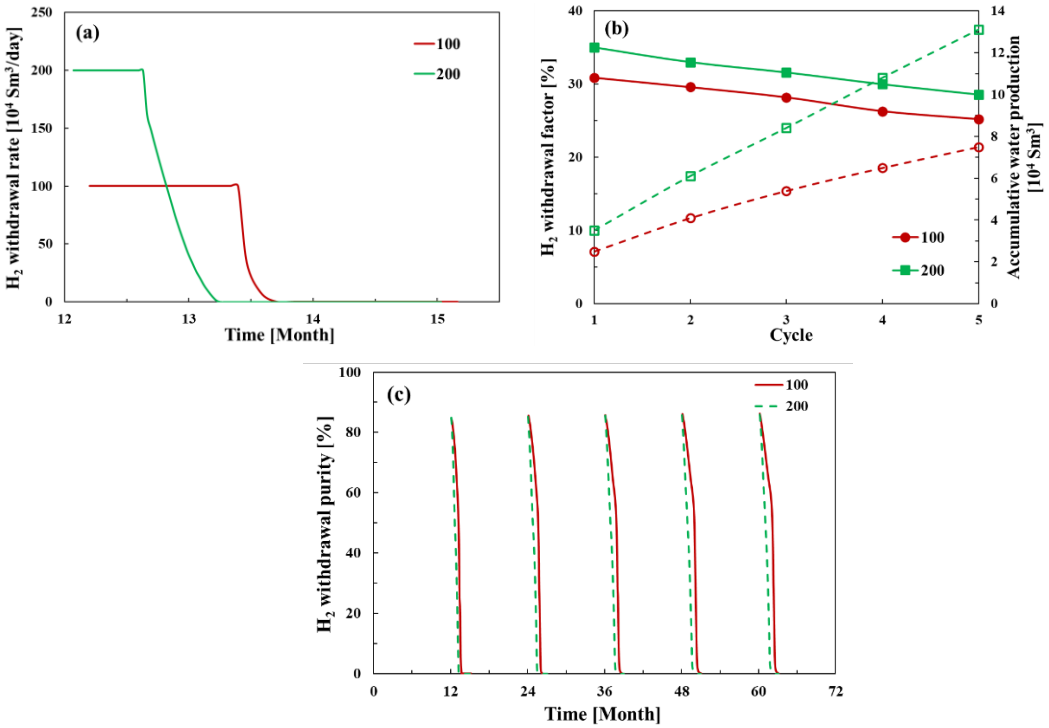

Figure 4. Effect of the prescribed H_2 withdrawal rate on (a) actual H_2 withdrawal rate during the 1st withdrawal cycle, (b) H_2 withdrawal factor and (c) H_2 withdrawal purity for the case of relative permeability hysteresis and brine contact angle of 51°.

Clearly, a larger prescribed H_{2-WR} causes the actual H_{2-WR} to deviate from the pre-set value and reach zero earlier in the simulated cases, **Figure 4(a) and (b)**. For example, during the 1st H_2 withdrawal cycle (for the prescribed $H_{2-WR} = 100 \times 10^4$ Sm^3/day and $H_{2-WR} = 200 \times 10^4$ Sm^3/day), the actual H_{2-WR} started to deviate from the prescribed value on the 38th and 18th day, respectively, while it reached zero on the 50th and 36th day, respectively. This is due to the faster pressure depletion caused by the larger H_{2-WR} [48]. Therefore, it is suggested that sufficient H_2 is stored and sufficiently high reservoir pressure is maintained for continuous H_2 withdrawal at an expected withdrawal rate. Furthermore, a larger H_{2-WR} caused a larger H_{2-WF} and a more serious water production problem. For example, for the prescribed $H_{2-WR} = 100 \times 10^4$ Sm^3/day and $H_{2-WR} = 200 \times 10^4$ Sm^3/day, by the end of the 5th H_2

withdrawal cycle, H_{2-WF} was 25% and 29% respectively, and cumulative water production reached 7.5 $\times$ 10^4 Sm^3 and 13.1 $\times$ 10^4 Sm^3, respectively.

In principle, larger H_2 injection rates result in higher viscous forces, which can override capillary forces (analogue to CO_2 flooding [49]), and suppress lateral H_2 migration beneath the caprock, resulting in a larger H_{2-WF} [31]. However, to avoid water production problems, an optimized H_2 withdrawal rate is required; to determine this optimum H_2 withdrawal scheme, it is suggested that a balance between initial gas in place, transient H_2 demand, and gas purification/separation ability should all be considered [23].

3.3 Impact of gas type

During the past decades, CGS has been investigated comprehensively (e.g., [31,40,42,43,50–54]). In contrast, UHS is a relatively new technology which is still in its infancy [27,55–57]. Whether previous learnings from CGS can be directly used in UHS is still uncertain. Therefore, in this section, UHS and CGS are compared (under the prescribed gas withdrawal rate of 100 $\times$ 10^4 Sm^3/day and RPH conditions, **Table 3** and **Figure 5**.

Table 3. Comparisons between underground hydrogen storage (UHS) and CO_2 geo-storage (CGS) during the first cycle of withdrawal, under the prescribed gas withdrawal rate of 100 $\times$ 10^4 Sm^3/day and relative permeability hysteresis conditions.

Gas	Plume areal coverage	Deviation from the prescribed withdrawal rate	Withdrawal factor by the end	Withdrawal purity at the beginning
UHS	Large: 35.22 km^2; 30.5%	Early: 38 days	Low: 31%	Low: 84%
CGS	Small: 14.58 km^2; 12.6%	Late: 50 days	High: 44%	High: 96%

248

249

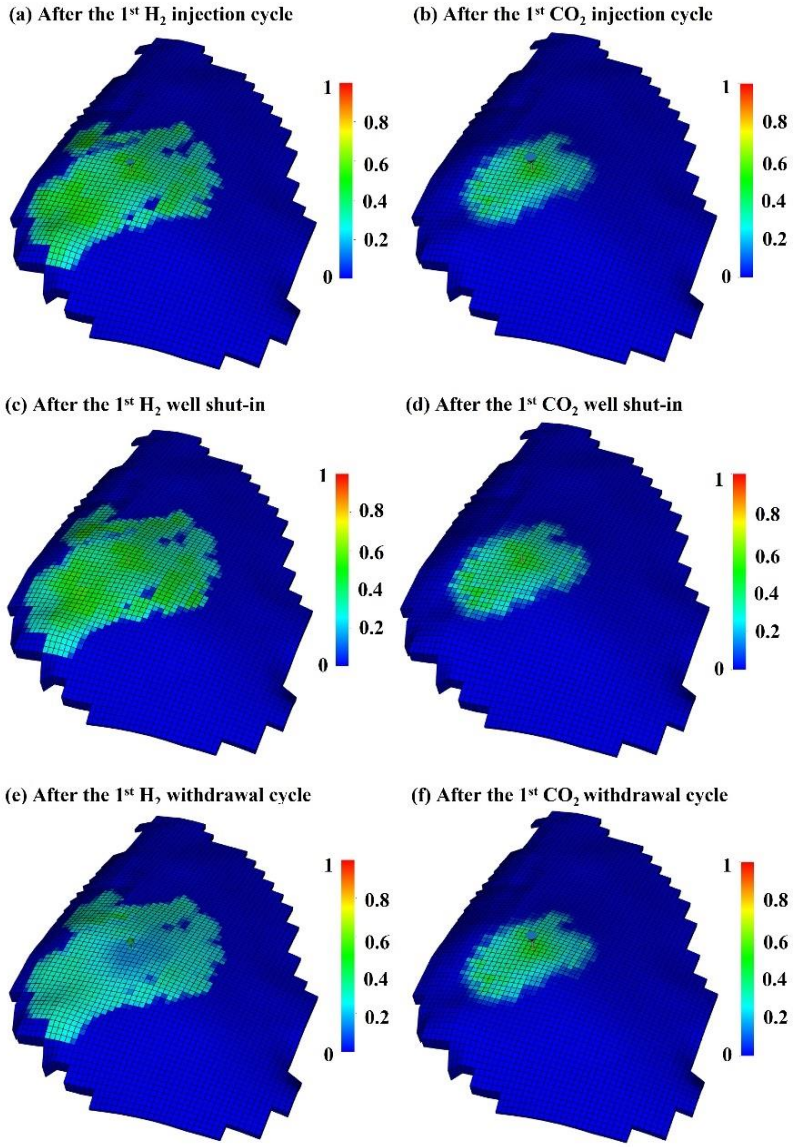

250

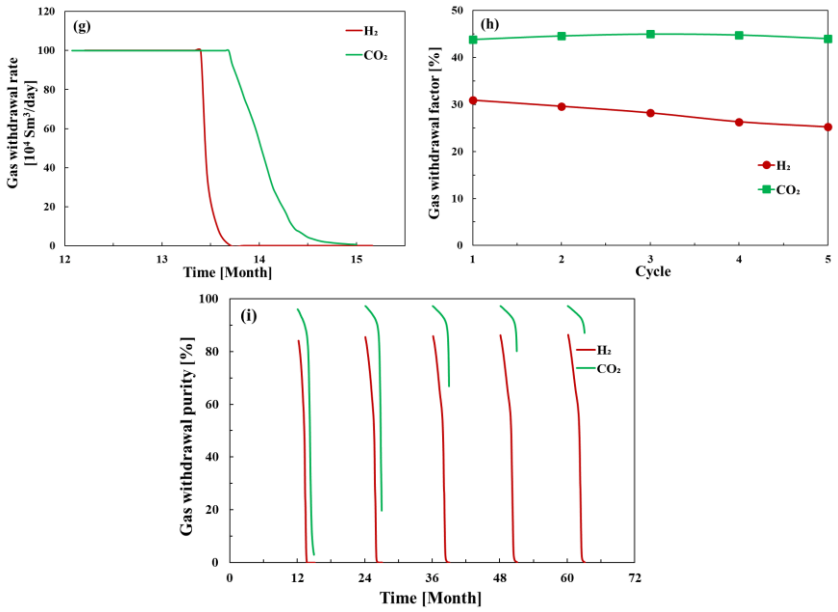

Figure 5. (a-f) Gas saturation distribution during the 1st H_2 storage cycle; (g) the actual gas withdrawal rate during the 1st withdrawal cycle; (h) gas withdrawal factor during the continuous 5 withdrawal cycles and (i) gas withdrawal purity during the continuous 5 withdrawal cycles under the prescribed withdrawal rate of 100×10^4 Sm^3/day and relative permeability hysteresis conditions.

Clearly, UHS and CGS exhibit significant differences in gas saturation distribution, actual gas withdrawal rate, gas withdrawal factor and gas purity, **Table 3** and **Figure 5**. After the initial gas injection for 9 months, the H_2 plume was ~ 2 - 5 times larger than CO_2, **Figure 5(a)** and **(b)** - this difference is caused by different gas viscosity and diffusivity [27]; after a well shut-in for 3 months, H_2 migrated significantly upward and accumulated beneath the caprock, while CO_2 only migrated slightly upward, **Figure 5(c)** and **(d)** - this was mainly caused by the difference in gas-brine density [27,58]. Furthermore, as shown in **Table 3**, **Figure 5(h) and (i)**, in the same timeframe, H_{2-WF} and H_{2-WP} were smaller than CO_{2-WF} and CO_{2-WP}.

Note that sandstone rocks are more water-wet in a H_2 environment than in a CO_2 environment [55,57,59,60], therefore gas bubble snap-off is more favored for H_2 than

for CO_2, which has led lower H_{2-WF} than CO_{2-WF} [61,62]). Meanwhile, especially during the gas injection stage, viscous fingering was predicted to be more pronounced for H_2 than for CO_2 [27], and that H_2 moves farther away from the wellbore region than CO_2 [57].

4 Conclusions and Recommendations

Underground hydrogen storage (UHS) is a promising technology which could aid the development of a large-scale hydrogen economy [12–17]. For UHS in saline aquifers, H_2-multi-cycle injection/withdrawal schemes are influenced by the energy supply and demand [23,63]. H_2-brine two phase flow physics, and H_2-brine-rock interactions determine UHS performance [7,27]. Therefore, in this work, the impact of relative permeability hysteresis, rock wettability, and injection/withdrawal schemes are systematically studied, and the results for UHS are then compared with those for CO_2 geo-storage (CGS). The following conclusions are reached:

1) H_2-brine relative permeability hysteresis results in a lower H_2 withdrawal factor, but a higher purity of withdrawn gas.
2) More water-wet rocks have lower H_2 withdrawal efficiencies.
3) Larger H_2 withdrawal rates increase H_2 withdrawal efficiency, but also increase water production.
4) UHS and CGS demonstrate significant differences and direct correlations should be avoided.

This study provides important information to aid in the implementation of a large-scale hydrogen economy, and therefore also supports the decarbonization of energy supply chains. For future work, it is suggested to further analyze the pore-scale H_2-brine two phase flow physics, and to establish a better understanding of meso-scale parameters (such as the H_2-brine relative permeabilities for cyclic drainage and imbibition processes and how they vary with wettability). Such improved input data leads directly to improved prediction of UHS performance [64,65].

Acknowledgements

Bin Pan thanks the initiative funding from the University of Science and Technology Beijing. Weiyao Zhu thanks the funding support from the National Natural Science Foundation of China (No. 51974013 and No. 11372033) and Open Research Foundation (NEPU-EOR-2019-003). Yang Ju acknowledges the funding support from the National Natural Science Foundation of China (No. 52121003). Christopher R. Clarkson thanks the sponsors of the Tight Oil Consortium (TOC) and Ovintiv and Shell for support of his Chair position in Unconventional Gas and Light Oil Research in the Department of Geoscience at the University of Calgary. Stefan Iglauer would like to thank the Australian Research Council for financial support (under grant DP220102907).

References

[1] Hosseini SE, Wahid MA. Hydrogen production from renewable and sustainable

energy resources: Promising green energy carrier for clean development. Renew Sustain Energy Rev 2016;57:850–66. https://doi.org/10.1016/J.RSER.2015.12.112.

[2] Lau LC, Lee KT, Mohamed AR. Global warming mitigation and renewable energy policy development from the Kyoto Protocol to the Copenhagen Accord—A comment. Renew Sustain Energy Rev 2012;16:5280–4. https://doi.org/10.1016/J.RSER.2012.04.006.

[3] Lam PTI, Law AOK. Crowdfunding for renewable and sustainable energy projects: An exploratory case study approach. Renew Sustain Energy Rev 2016;60:11–20. https://doi.org/10.1016/J.RSER.2016.01.046.

[4] Rourke FO, Boyle F, Reynolds A. Renewable energy resources and technologies applicable to Ireland. Renew Sustain Energy Rev 2009;13:1975–84. https://doi.org/10.1016/J.RSER.2009.01.014.

[5] Bhuiyan MRA, Mamur H, Begum J. A brief review on renewable and sustainable energy resources in Bangladesh. Clean Eng Technol 2021;4:100208. https://doi.org/10.1016/J.CLET.2021.100208.

[6] Widén J, Carpman N, Castellucci V, Lingfors D, Olauson J, Remouit F, et al. Variability assessment and forecasting of renewables: A review for solar, wind, wave and tidal resources. Renew Sustain Energy Rev 2015;44:356–75. https://doi.org/10.1016/J.RSER.2014.12.019.

[7] Heinemann N, Alcalde J, Miocic JM, Hangx SJT, Kallmeyer J, Ostertag-Henning C, et al. Enabling large-scale hydrogen storage in porous media – the

scientific challenges. Energy Environ Sci 2021;14:853–64. https://doi.org/10.1039/d0ee03536j.

[8] Thaysen EM, McMahon S, Strobel GJ, Butler IB, Ngwenya BT, Heinemann N, et al. Estimating microbial growth and hydrogen consumption in hydrogen storage in porous media. Renew Sustain Energy Rev 2021;151:111481. https://doi.org/10.1016/J.RSER.2021.111481.

[9] Miocic JM, Heinemann N, Edlmann K, Scafidi J, Molaei F, Alcalde J. Underground hydrogen storage: a review. Geol Soc London 2022;528.

[10] Rezaei A, Hassanpouryouzband A, Molnar I, Derikvand Z, Haszeldine S, Edlmann K. Relative permeability of hydrogen and aqueous brines in sandstones and carbonates at reservoir conditions. Geophys Res Lett 2022;49.

[11] Heinemann N, Scafidi J, Pickup G, Thaysen EM, Hassanpouryouzband A, Wilkinson M, et al. Hydrogen storage in saline aquifers: The role of cushion gas for injection and production. Int J Hydrogen Energy 2021;46:39284–96.

[12] Lankof L, Tarkowski R. Assessment of the potential for underground hydrogen storage in bedded salt formation. Int J Hydrogen Energy 2020;45:19479–92. https://doi.org/10.1016/j.ijhydene.2020.05.024.

[13] Tarkowski R. Underground hydrogen storage: Characteristics and prospects. Renew Sustain Energy Rev 2019;105:86–94. https://doi.org/10.1016/j.rser.2019.01.051.

[14] Tarkowski R, Czapowski G. Salt domes in Poland – Potential sites for hydrogen storage in caverns. Int J Hydrogen Energy 2018;43:21414–27.

https://doi.org/10.1016/J.IJHYDENE.2018.09.212.

[15] Ozarslan A. Large-scale hydrogen energy storage in salt caverns. Int J Hydrogen Energy 2012;37:14265–77. https://doi.org/10.1016/j.ijhydene.2012.07.111.

[16] Carden PO, Paterson L. Physical, chemical and energy aspects of underground hydrogen storage. Int J Hydrogen Energy 1979;4:559–69. https://doi.org/10.1016/0360-3199(79)90083-1.

[17] Qiu Y, Zhou S, Wang J, Chou J, Fang Y, Pan G, et al. Feasibility analysis of utilising underground hydrogen storage facilities in integrated energy system: Case studies in China. Appl Energy 2020;269:115140. https://doi.org/10.1016/j.apenergy.2020.115140.

[18] Sedev R, Akhondzadeh H, Ali M, Keshavarz A, Iglauer S. Contact Angles of a Brine on a Bituminous Coal in Compressed Hydrogen. Geophys Res Lett 2022;49:e2022GL098261. https://doi.org/10.1029/2022GL098261.

[19] Iglauer S, Akhondzadeh H, Abid H, Paluszny A, Keshavarz A, Ali M, et al. Hydrogen flooding of a coal core: Effect on Coal Swelling. Geophys Res Lett 2022;49:e2021GL096873. https://doi.org/10.1029/2021GL096873.

[20] Kanaani M, Sedaee B, Asadian-Pakfar M. Role of cushion gas on underground hydrogen storage in depleted oil reservoirs. J Energy Storage 2022;45:103783. https://doi.org/10.1016/J.EST.2021.103783.

[21] Amid A, Mignard D, Wilkinson M. Seasonal storage of hydrogen in a depleted natural gas reservoir. Int J Hydrogen Energy 2016;41:5549–58. https://doi.org/10.1016/j.ijhydene.2016.02.036.

[22] Sainz-Garcia A, Abarca E, Rubi V, Grandia F. Assessment of feasible strategies for seasonal underground hydrogen storage in a saline aquifer. Int J Hydrogen Energy 2017;42:16657–66. https://doi.org/10.1016/j.ijhydene.2017.05.076.

[23] Luboń K, Tarkowski R. Numerical simulation of hydrogen injection and withdrawal to and from a deep aquifer in NW Poland. Int J Hydrogen Energy 2020;45:2068–83. https://doi.org/10.1016/j.ijhydene.2019.11.055.

[24] Caglayan DG, Weber N, Heinrichs HU, Linßen J, Robinius M, Kukla PA, et al. Technical potential of salt caverns for hydrogen storage in Europe. Int J Hydrogen Energy 2020;45:6793–805. https://doi.org/10.1016/J.IJHYDENE.2019.12.161.

[25] Portarapillo M, Di Benedetto A. Risk assessment of the large-scale hydrogen storage in salt caverns. Energies 2021, 14, 2856 2021;14:2856. https://doi.org/10.3390/EN14102856.

[26] Walters AB, Walters, B. A. Technical and environmental aspects of underground hydrogen storage. Whe2 1976;2:2B_65-2B_79.

[27] Pan B, Yin X, Ju Y, Iglauer S. Underground hydrogen storage: influencing parameters and future outlook. Adv Colloid Interface Sci 2021， 294， 102473.

[28] Pfeiffer WT, Bauer S. Subsurface Porous Media Hydrogen Storage – Scenario Development and Simulation. Energy Procedia 2015;76:565–72. https://doi.org/10.1016/J.EGYPRO.2015.07.872.

[29] Pfeiffer WT, Beyer C, Bauer S. Hydrogen storage in a heterogeneous sandstone formation: Dimensioning and induced hydraulic effects. Pet Geosci

2017;23:315–26. https://doi.org/10.1144/PETGEO2016-050/CITE/REFWORKS.

[30] Feldmann F, Hagemann B, Ganzer L, Panfilov M. Numerical simulation of hydrodynamic and gas mixing processes in underground hydrogen storages. Environ Earth Sci 2016;75:1–15. https://doi.org/10.1007/S12665-016-5948-Z/FIGURES/9.

[31] Juanes R, Spiteri EJ, Orr FM, Blunt MJ. Impact of relative permeability hysteresis on geological CO_2 storage. Water Resour Res 2006;42:12418. https://doi.org/10.1029/2005WR004806.

[32] Pan B, Ni T, Zhu W, Yang Y, Ju Y, Zhang L, et al. Mini review on wettability in the methane-liquid-rock system at reservoir conditions: Implications for gas recovery and geo-storage. Energy & Fuels 2022;36:4268–75.

[33] Aziz K, A S. Petroleum reservoir simulation. 1979.

[34] Floris FJT, Bush MD, Cuypers M, Roggero F, Syversveen AR. Methods for quantifying the uncertainty of production forecasts: A comparative study. Pet Geosci 2001;7:S87–96. https://doi.org/10.1144/PETGEO.7.S.S87/CITE/REFWORKS.

[35] Yekta AE, Manceau JC, Gaboreau S, Pichavant M, Audigane P. Determination of hydrogen–water relative permeability and capillary pressure in sandstone: Application to underground hydrogen injection in sedimentary Formations. Transp Porous Media 2018;122:333–56. https://doi.org/10.1007/s11242-018-1004-7.

[36] Hashemi L, Blunt M, Hajibeygi H. Pore-scale modelling and sensitivity analyses of hydrogen-brine multiphase flow in geological porous media. Sci Reports 2021 111 2021;11:1–13. https://doi.org/10.1038/s41598-021-87490-7.

[37] Bachu S. Drainage and imbibition CO_2/brine relative permeability curves at in situ conditions for sandstone formations in western Canada. Energy Procedia, 37, 2013, 4428–36. https://doi.org/10.1016/j.egypro.2013.07.001.

[38] Bennion DB, Bachu S. Drainage and imbibition relative permeability relationships for supercritical CO_2/brine and H_2S/brine systems in intergranular sandstone, carbonate, shale, and anhydrite rocks. SPE Reserv Eval Eng 2008;11:487–96. https://doi.org/10.2118/99326-pa.

[39] Krevor SCM, Pini R, Zuo L, Benson SM. Relative permeability and trapping of CO_2 and water in sandstone rocks at reservoir conditions. Water Resour Res 2012;48. https://doi.org/10.1029/2011WR010859.

[40] Pan B, Li Y, Wang H, Jones F, Iglauer S. CO_2 and CH_4 wettabilities of organic-rich shale. Energy and Fuels 2018;32:1914–22. https://doi.org/10.1021/acs.energyfuels.7b01147.

[41] Pan B, Jones F, Huang Z, Yang Y, Li Y, Hejazi SH, et al. Methane (CH_4) wettability of clay-coated quartz at reservoir conditions. Energy and Fuels 2019;33:788–95. https://doi.org/10.1021/acs.energyfuels.8b03536.

[42] Iglauer S, Pentland CH, Busch A. CO_2 wettability of seal and reservoir rocks and the implications for carbon geo-sequestration. Water Resour Res 2015;51:729–74. https://doi.org/10.1002/2014WR015553.

447 [43] Iglauer S, Paluszny A, Pentland CH, Blunt MJ. Residual CO_2 imaged with X-ray
448 micro-tomography. Geophys Res Lett 2011;38:n/a-n/a.
449 https://doi.org/10.1029/2011GL049680.
450 [44] Hu R, Wan J, Kim Y, Tokunaga TK. Wettability impact on supercritical CO_2
451 capillary trapping: Pore-scale visualization and quantification. Water Resour Res
452 2017;53:6377–94. https://doi.org/10.1002/2017WR020721.
453 [45] Hu R, Wan J, Yang Z, Chen Y, Tokunaga T. Wettability and flow rate impacts on
454 immiscible displacement: A theoretical model. Geophys Res Lett 2018;45:3077–
455 86. https://doi.org/10.1002/2017GL076600.
456 [46] Pan B, Clarkson CR, Younis A, Song C, Debuhr C, Ghanizadeh A, et al.
457 Fracturing fluid loss in unconventional reservoirs: evaluating the impact of
458 osmotic pressure and surfactant and methods to upscale results. URTeC Tech
459 2021:26–8. https://doi.org/10.15530/URTEC-2021-5139.
460 [47] Pan B, Clarkson CR, Younis A, Song C, Debuhr C, Ghanizadeh A, et al. New
461 methods to evaluate impacts of osmotic pressure and surfactant on fracturing
462 fluid loss and effect of contact angle on spontaneous imbibition data scaling in
463 unconventional reservoirs. Fuel 2022;328.
464 https://doi.org/10.1016/j.fuel.2022.125328.
465 [48] Clarkson CR. Unconventional reservoir rate-transient analysis. Elsevier; 2021.
466 [49] Jin X, Chao C, Edlmann K, Fan X. Understanding the interplay of capillary and
467 viscous forces in CO_2 core flooding experiments. J Hydrol 2022;606:127411.
468 [50] Wan J, Kim Y, Tokunaga TK. Contact angle measurement ambiguity in

supercritical CO_2-water-mineral systems: Mica as an example. Int J Greenh Gas Control 2014;31:128–37. https://doi.org/10.1016/j.ijggc.2014.09.029.

[51] Wan J, Tokunaga TK, Ashby PD, Kim Y, Voltolini M, Gilbert B, et al. Supercritical CO_2 uptake by nonswelling phyllosilicates. Proc Natl Acad Sci U S A 2018;115:873–8. https://doi.org/10.1073/pnas.1710853114.

[52] Iglauer S. CO_2-water-rock wettability: Variability, influencing factors, and implications for CO_2 geostorage. Acc Chem Res 2017;50:1134–42. https://doi.org/10.1021/acs.accounts.6b00602.

[53] Pan B, Gong C, Wang X, Li Y, Iglauer S. The interfacial properties of clay-coated quartz at reservoir conditions. Fuel 2020;262:116461. https://doi.org/10.1016/j.fuel.2019.116461.

[54] Tenney CM, Cygan RT. Molecular simulation of carbon dioxide, brine, and clay mineral interactions and determination of contact angles. Environ Sci Technol 2014;48:2035–42. https://doi.org/10.1021/es404075k.

[55] Ali M, Pan B, Yekeen N, Al-Anssari S, Al-Anazi A, Keshavarz A, et al. Assessment of wettability and rock-fluid interfacial tension of caprock: Implications for hydrogen and carbon dioxide geo-storage. Int J Hydrogen Energy 2022. https://doi.org/10.1016/J.IJHYDENE.2022.02.149.

[56] Pan B, Yin X, Iglauer S. Rock-fluid interfacial tension at subsurface conditions: Implications for H_2, CO_2 and natural gas geo-storage. Int J Hydrogen Energy 2021. https://doi.org/10.1016/j.ijhydene.2021.05.067.

[57] Pan B, Yin X, Zhu W, Yang Y, Ju Y, Yuan Y, et al. Theoretical study of brine

491 secondary imbibition in sandstone reservoirs: Implications for H_2, CH_4, and CO_2
492 geo-storage. Int J Hydrogen Energy 2022;47:18058–66.
493 https://doi.org/10.1016/J.IJHYDENE.2022.03.275.
494 [58] Ren B, Jerry J, Duncan I, Lake L. Buoyant flow of H_2 versus CO_2 in storage
495 aquifers. SPE Annu. Tech. Conf. Exhib. Houston, Texas, USA, Oct. 2022.
496 [59] Iglauer S, Ali M, Keshavarz A. Hydrogen wettability of sandstone reservoirs:
497 Implications for hydrogen geo-storage. Geophys Res Lett 2020.
498 https://doi.org/10.1029/2020GL090814.
499 [60] Ali M, Jha NK, Al-Yaseri A, Zhang Y, Iglauer S, Sarmadivaleh M. Hydrogen
500 wettability of quartz substrates exposed to organic acids; Implications for
501 hydrogen geo-storage in sandstone reservoirs. J Pet Sci Eng 2021;207:109081.
502 https://doi.org/10.1016/J.PETROL.2021.109081.
503 [61] Krevor S, Blunt MJ, Benson SM, Pentland CH, Reynolds C, Al-Menhali A, et al.
504 Capillary trapping for geologic carbon dioxide storage – From pore scale physics
505 to field scale implications. Int J Greenh Gas Control 2015;40:221–37.
506 https://doi.org/10.1016/J.IJGGC.2015.04.006.
507 [62] Lysyy M, Ersland G, Fernø M. Pore-scale dynamics for underground porous
508 media hydrogen storage. Adv Water Resour 2022;163:104167.
509 https://doi.org/10.1016/J.ADVWATRES.2022.104167.
510 [63] Lysyy M, Fernø M, Ersland G. Seasonal hydrogen storage in a depleted oil and
511 gas field. Int J Hydrogen Energy 2021;46:25160–74.
512 https://doi.org/10.1016/J.IJHYDENE.2021.05.030.

513 [64] Tarkowski R, Uliasz-Misiak B. Towards underground hydrogen storage: A
514 review of barriers. Renew Sustain Energy Rev 2022;162:112451.
515 https://doi.org/10.1016/J.RSER.2022.112451.
516 [65] van Rooijen W, Hashemi L, Boon M, Farajzadeh R, Hajibeygi H. Microfluidics-
517 based analysis of dynamic contact angles relevant for underground hydrogen
518 storage. Adv Water Resour 2022;164:104221.
519 https://doi.org/10.1016/J.ADVWATRES.2022.104221.
520